

Article

Activated Carbon, Carbon Nanofiber and Carbon Nanotube Supported Molybdenum Carbide Catalysts for the Hydrodeoxygenation of Guaiacol

Eduardo Santillan-Jimenez, Maxime Perdu, Robert Pace, Tonya Morgan and Mark Crocker *

University of Kentucky Center for Applied Energy Research, 2540 Research Park Drive, Lexington, KY 40511, USA; E-Mails: e.santillan@uky.edu (E.S.-J.); maximeperdu@yahoo.fr (M.P.); robert.pace@uky.edu (R.P.); tonya.morgan@uky.edu (T.M.)

* Author to whom correspondence should be addressed; E-Mail: mark.crocker@uky.edu; Tel.: +1-859-257-0295; Fax: +1-859-257-0302.

Academic Editor: Keith Hohn

Received: 15 December 2014 / Accepted: 10 March 2015 / Published: 16 March 2015

Abstract: Molybdenum carbide was supported on three types of carbon support—activated carbon; multi-walled carbon nanotubes; and carbon nanofibers—using ammonium molybdate and molybdic acid as Mo precursors. The use of activated carbon as support afforded an X-ray amorphous Mo phase, whereas crystalline molybdenum carbide phases were obtained on carbon nanofibers and, in some cases, on carbon nanotubes. When the resulting catalysts were tested in the hydrodeoxygenation (HDO) of guaiacol in dodecane, catechol and phenol were obtained as the main products, although in some instances significant amounts of cyclohexane were produced. The observation of catechol in all reaction mixtures suggests that guaiacol was converted into phenol via sequential demethylation and HDO, although the simultaneous occurrence of a direct demethoxylation pathway cannot be discounted. Catalysts based on carbon nanofibers generally afforded the highest yields of phenol; notably, the only crystalline phase detected in these samples was Mo₂C or Mo₂C- ζ , suggesting that crystalline Mo₂C is particularly selective to phenol. At 350 °C, carbon nanofiber supported Mo₂C afforded near quantitative guaiacol conversion, the selectivity to phenol approaching 50%. When guaiacol HDO was performed in the presence of acetic acid and furfural, guaiacol conversion decreased, although the selectivity to both catechol and phenol was increased.

Keywords: activated carbon; carbon nanofibers; carbon nanotubes; molybdenum; carbide catalysts; hydrodeoxygenation; guaiacol; bio-oil upgrading

1. Introduction

Lignin is a complex biopolymer which is produced as a waste product by the pulp and paper industry and is typically burned on-site to operate factory processes [1]. In lieu of simply combusting this valuable source of aromatics and phenolics, various depolymerization [2] and densification [3] strategies are under development with the goal of producing value-added liquid fuels and chemicals from the lignin polymer. However, many of the products obtained from these processes require further upgrading in the form of deoxygenation before they can be utilized as fuels. In order to simplify laboratory deoxygenation studies, model compounds are typically used as surrogates for the products obtained from lignin depolymerization, guaiacol being one of the most widely used models. Guaiacol possesses both phenolic and methoxy moieties which are present throughout lignin, and affords the opportunity to examine the selectivity toward hydrogenation/hydrogenolysis of the -OH and -OCH₃ functionalities *versus* the aromatic ring [4–6]. Guaiacol is also more representative of actual lignin product streams than other simple model compounds due to its greater propensity for coking and its tendency to be more refractory towards hydrodeoxygenation (HDO) than other common lignin models [7].

A variety of catalytic approaches have been examined in an effort to produce fuel-like compounds from oxygenates derived from lignocellulosic sources, HDO being the most widely applied. Typically, sulfided Co-Mo and Ni-Mo [8,9] catalysts, as well as supported precious metals [6], are employed for this purpose. While effective, sulfided catalysts suffer from deactivation in the absence of additional sulfur and can lead to product contamination through sulfur leaching. Given these drawbacks, systems utilizing supported precious metals have been examined as an alternative. However, these catalysts show strong selectivity for ring hydrogenation processes in addition to hydrodeoxygenation. Ring hydrogenation is somewhat undesirable in that it destroys the aromatic character of the compounds produced. Coupled with the often prohibitive cost of precious metals and increased hydrogen consumption resulting from ring hydrogenation, current catalytic strategies leave considerable room for improvement.

Given the stability and platinum-like catalytic behavior of transition metal carbides [10], these materials seem to be a logical alternative for catalyzing deoxygenation reactions. In fact, various unsupported molybdenum carbides have been shown to possess high catalytic activity in hydrocarbon conversion reactions, this being a consequence of metal-carbon bond interactions that yield a noble metal like d-state density around the Fermi level [11]. However, bulk carbides possess intrinsically low surface areas, in addition to requiring the use of highly flammable carburization gases such as methane in their synthesis. Consequently, metal carbides supported on high surface area substrates, including carbon nanomaterials, have been examined in order to enhance the catalytic properties of these formulations. Carbon-based supports are particularly attractive given that the substrate is capable of acting as the carbon source in the synthesis of the catalyst, eliminating the need for carburization gases. Indeed, metal carbides supported on activated carbon (AC) [12,13], ordered mesoporous carbon (OMC) [14], carbon

nanofibers (CNF) [2,15–17] and carbon nanotubes (CNT) [18] have already shown promising activity and stability in the deoxygenation of biomass-derived molecules. The performance of these supported carbides is in most cases superior to that of the bulk molybdenum carbide as a result of improved active site accessibility through greater dispersion of carbide phases on the carbon supports [12]. Herein, we report a study of guaiacol hydrodeoxygenation using molybdenum carbides supported on three types of carbon carrier, namely activated carbon, multi-walled carbon nanotubes, and carbon nanofibers. The effectiveness and material properties of each catalyst were assessed in an attempt to gain insights into structure-activity relationships with the specific goal of identifying the carbide phases and/or supports which provide optimal HDO activity.

2. Results and Discussion

2.1. Catalyst Characterization

Synthesized catalysts—the names of which in this article are composed of a Mo loading (7.5 or 20 wt.%), a Mo precursor (Am or Ac representing ammonium molybdate and molybdic acid, respectively), and a carbon support (AC, CNF or CNT)—were analyzed via XRD in an effort to confirm the formation of crystalline molybdenum-containing phases (including molybdenum carbide phases) and measure the corresponding particle sizes. Figure 1 shows the X-ray diffractograms of representative catalysts showing distinct Mo-containing phases, while Table 1 summarizes the Mo-containing phases detected in each catalyst and provides the average particle size for each crystalline phase detected. In contrast to previous reports [12], molybdenum carbides supported on activated carbon demonstrated no crystalline phases under XRD analysis even when prepared at high temperature (1000 °C). This suggests the formation of a highly dispersed Mo-containing phase on the activated carbon support employed.

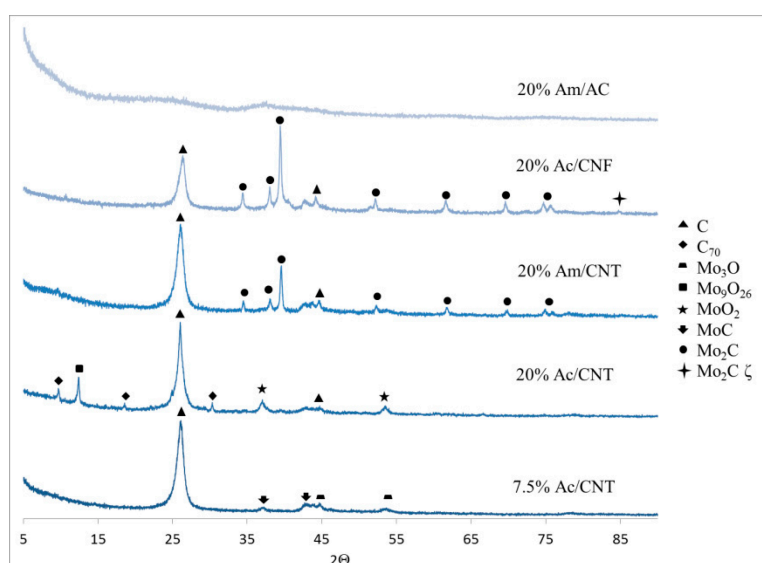


Figure 1. X-ray diffractograms of representative catalysts showing different crystalline phases.

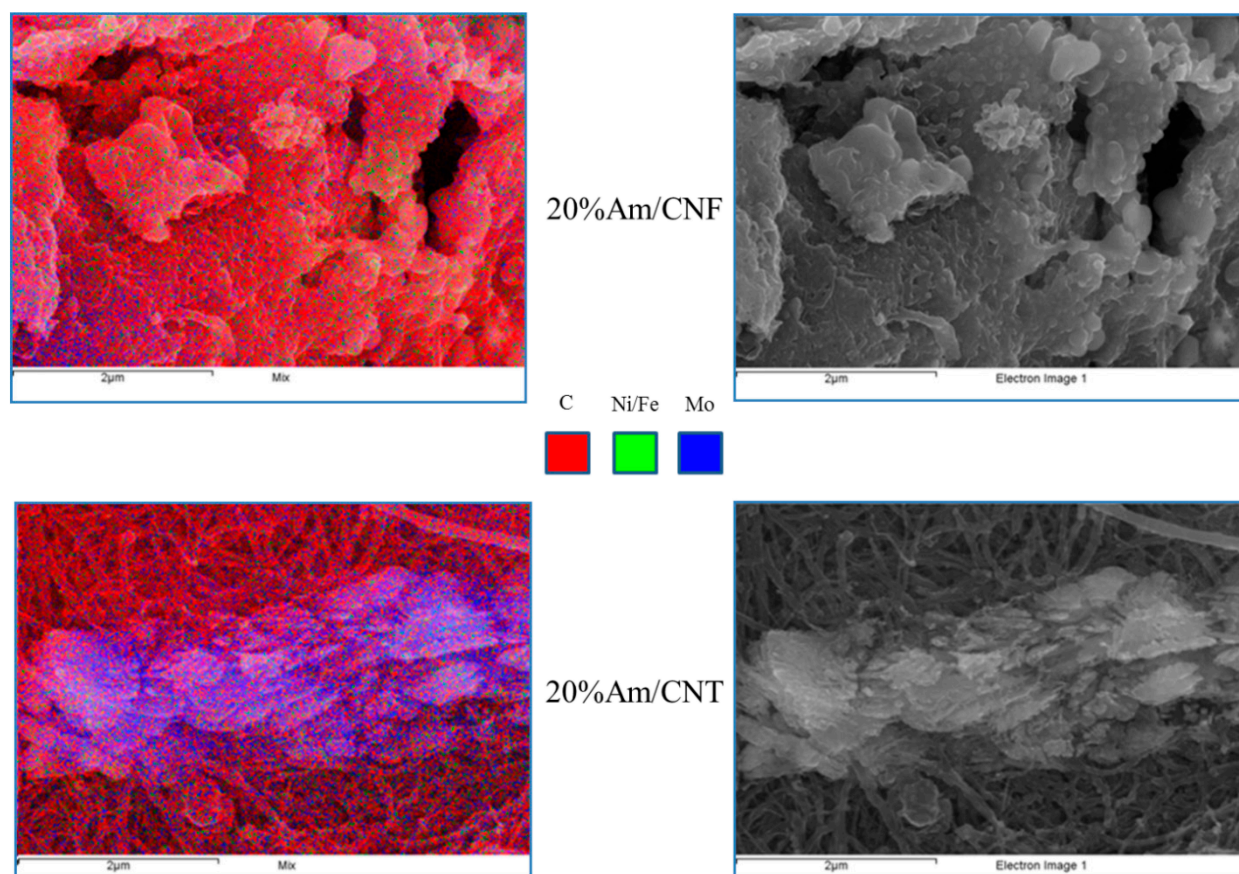
Table 1. Type and average particle size of the Mo-containing phases in each catalyst as determined by XRD.

Catalyst	Crystalline phases detected	Average particle size (nm)
7.5% Ac/AC	None	-
20% Ac/AC	None	-
7.5% Am/AC	None	-
20% Am/AC	None	-
7.5% Ac/CNF	Mo ₂ C & MoC	Mo ₂ C: 13.8 & MoC: 13.0
20% Ac/CNF	Mo ₂ C- ζ (zeta)	16.1
7.5% Am/CNF	Mo ₂ C	12.6
20% Am/CNF	Mo ₂ C	11.3
7.5% Ac/CNT	MoC & Mo ₃ O	MoC: 13.3 & Mo ₃ O: 6.3
20% Ac/CNT	MoO ₂ & Mo ₉ O ₂₆	MoO ₂ : 8.8 & Mo ₉ O ₂₆ : 9.2
7.5% Am/CNT	None	-
20% Am/CNT	Mo ₂ C- ζ (zeta)	16.2

The textural properties of the catalysts were measured by means of nitrogen physisorption, the results of these measurements being summarized in Table 2, which also includes the corresponding data for the carbon supports employed in this study. Interestingly, little change in pore size distribution occurs after carburization of the activated carbon and carbon nanofiber supported catalysts, while a significant increase in macroporosity occurs for the carbon nanotube supported catalysts. The accompanying increase in pore volume and decrease in surface area is likely a result of the agglomeration of large molybdenum particles ($>2 \mu\text{m}$) which were found to be present only in the carbon nanotube supported catalysts as demonstrated in Figure 2. Indeed, large ($\sim 2 \mu\text{m}$) molybdenum carbide particles were observed in all the micrographs of the CNT supported catalysts containing Mo₂C or MoC, these microparticles being absent from the CNF supported formulations in which molybdenum carbide was exclusively present in the form of nanoparticles (see Figure 2). Given that the *average* particle size of molybdenum carbide is relatively similar in both CNT and CNF supported catalysts (see Table 1), it can be concluded that the use of CNT as support results in a bimodal particle size distribution containing both micro and nanoparticles, whereas the use of CNF affords solely well dispersed nanoparticles. These conclusions are also supported by SEM-EDX mapping, which reveals homogenous molybdenum dispersion throughout the CNF, as well as a uniform structural morphology even at higher magnification. In contrast, the CNT supported carbides demonstrate both a dispersed molybdenum phase on the nanotubes as well as a bulk phase which forms as an agglomeration around the nanotubes. The difference in Mo₂C morphology between the CNF and CNT supports can be rationalized on the basis of the much lower surface area and mesopore volume of the CNT support, *i.e.*, at the 20 wt.% Mo loading the surface area of the CNT support is evidently insufficient to stabilize all of the formed Mo₂C in a nanodisperse state.

Table 2. Textural properties of the synthesized catalysts and of the corresponding carbon supports.

Carbon support or catalyst	BET surface area ($\text{m}^2 \text{g}^{-1}$)	Pore volume ($\text{cm}^3 \text{g}^{-1}$)	Avg. pore diameter (nm)	Pore size distribution (%)		
				Micro	Meso	Macro
AC	1330	1.00	3.4	37	61	2
7.5% Ac/AC	781	0.60	3.6	36	63	1
20% Ac/AC	624	0.49	3.7	34	65	1
7.5% Am/AC	798	0.60	3.5	36	63	1
20% Am/AC	755	0.56	3.6	35	64	1
CNF	198	0.45	10.8	5	90	5
7.5% Ac/CNF	191	0.42	9.7	5	90	5
20% Ac/CNF	163	0.38	9.2	6	86	8
7.5% Am/CNF	165	0.38	10.7	4	94	2
20% Am/CNF	144	0.33	10	5	92	3
CNT	98	0.18	8.8	4	58	38
7.5% Ac/CNT	66	0.28	9.6	3	51	46
20% Ac/CNT	71	0.26	11.2	2	49	49
7.5% Am/CNT	69	0.36	12.5	2	43	55
20% Am/CNT	55	0.22	10.5	2	49	49

**Figure 2.** Scanning electron micrographs of 20% Am/CNF and 20% Am/CNT: EDX analysis (**left**) and backscattered electron images (**right**).

2.2. Catalyst Evaluation

2.2.1. Catalyst Evaluation in Water

The synthesized catalysts—as well as the bare supports—were first tested for activity in the upgrading of guaiacol in an aqueous environment. However, under these conditions the extent of guaiacol deoxygenation was low, catechol being the main reaction product (see Table S1 of the Supplementary Materials accompanying this article). Moreover, the results obtained did not reveal any significant trends, making it impossible to elucidate structure-activity relationships. Indeed, in some cases the bare carbon supports afforded better results in terms of conversion and/or selectivity than the corresponding molybdenum-containing catalysts. Therefore, the catalysts were tested in an organic environment in an effort to obtain more informative results.

2.2.2. Catalyst Evaluation in Dodecane

Table 3 summarizes the results of experiments performed to evaluate the synthesized catalysts and the bare supports in the upgrading of guaiacol in dodecane.

Table 3. Guaiacol upgrading in dodecane over different catalysts ^a.

Catalyst	Guaiacol conversion (%)	Selectivity to [Yield of] catechol (%)	Selectivity to [Yield of] phenol (%)	Gravimetric mass balance ^b (%)
None	7	15 [1]	0 [0]	98
AC	12	10 [1.2]	3 [0.4]	99
7.5% Ac/AC	26	21 [5.5]	12 [3.1]	98
20% Ac/AC	61	7 [4]	9 [6]	70
7.5% Am/AC	37	20 [7.4]	1 [0.4]	98
20% Am/AC	53	31 [16]	3 [2]	95
CNF	6	19 [1]	3 [0.2]	97
7.5% Ac/CNF	40	8 [0.3]	12 [4.8]	85
20% Ac/CNF	56	9 [5]	35 [20]	96
7.5% Am/CNF	33	9 [3]	38 [12]	98
20% Am/CNF	53	11 [5.8]	37 [20]	96
CNT	16	11 [1.8]	2 [0.3]	97
7.5% Ac/CNT	72	36 [26]	3 [2]	95
20% Ac/CNT	91	24 [22]	5 [4]	98
7.5% Am/CNT	33	33 [11]	3 [1]	97
20% Am/CNT	24	9 [2]	36 [8.6]	96
GNT	13	17 [2.2]	4 [0.5]	97

^a Reaction conditions: 0.125 g catalyst, 1.25 g guaiacol, 11.25 g dodecane, 300 °C, 580 psi of H₂, 4 h. ^b Mass balances were calculated considering only liquids and solids at the start and the end of the reaction, *i.e.*, mass balance = 100 × (mass of starting reaction mixture)/(mass of recovered liquids and solids). Gaseous reactants and products were omitted from the mass balance calculation for the reasons enumerated in Section 3.5.3.

Albeit the conversion and selectivity values observed in the experiment performed without catalyst can be attributed to thermal effects, it is interesting to note that some of the bare carbon supports display additional activity. Given that carbon nanofibers and carbon nanotubes are respectively grown using Ni and Fe catalysts and that the hydrodeoxygenation of guaiacol has been reported to proceed over both Ni [19–21] and Fe [22–24] catalysts, the activity of the bare supports could conceivably be caused by the residual presence of these metals. Indeed, the Ni and Fe content of the carbon supports was measured by means of Inductively Coupled Plasma-Optical Emission Spectrometry (ICP-OES) and determined to be non-negligible, as shown in Table 4.

Table 4. Results of ICP-OES analysis of the carbon supports used in this study.

Carbon support	Fe content	Ni content
AC	5022 ppm	666 ppm
CNF	334 ppm	1.9%
CNT	2.35%	40 ppm
GNT	837 ppm	18 ppm

However, the activity of Ni present in the CNF can be deemed to be minimal, since the conversion and selectivity values obtained using CNF are almost identical to those obtained in the blank (sans catalyst) run. Carbon nanotubes afforded higher guaiacol conversion than the blank run, albeit this cannot be entirely attributed to the presence of iron since a sample of graphitized nanotubes (GNT)—in which Fe content is reduced to 837 ppm by means of a thermal treatment (in helium) exceeding 2700 °C [25]—showed almost identical results (see Table 3). Similarly, the additional activity displayed by the bare supports relative to the blank run cannot be entirely attributed to the presence of acid sites on the surface of these materials since the graphitized nanotubes—in which these sites have been removed by the high temperatures employed during the graphitization process [26]—shows similar results (see Table 3). In a recent contribution by Jongerius *et al.*, the surface of the carbon supports in carbide catalysts were deemed inert since the high temperature employed in the carburization process effectively removes acidic functional groups from the supports [2]. However, the conversion and selectivity values obtained over graphitized nanotubes suggest that bare supports display some activity which must be taken into account during the interpretation of the results obtained using the Mo-containing catalysts.

Notably, in contrast with the results obtained in aqueous medium, higher guaiacol conversions were invariably obtained over the Mo-containing catalysts relative to the bare supports in an organic environment (using dodecane as solvent). The most abundant reaction products were typically catechol and phenol, albeit in some instances significant amounts of cyclohexane were produced (a more comprehensive account of the results of product analysis is given in Table S2 of the Supplementary Materials accompanying this article). The fact that catechol was observed in all reaction mixtures suggests that guaiacol is converted into phenol via sequential demethylation and HDO [7], which contrasts with the direct demethoxylation pathway proposed by Jongerius *et al.* [2], albeit the possibility for these two pathways to be operating in parallel cannot be discounted.

Among the aforementioned products—namely catechol, phenol, and cyclohexane—phenol represents the most desirable product, as it offers a good balance between depth of deoxygenation and value (an upgraded bio-oil or lignin depolymerization stream rich in catechol would still be unacceptably unstable

and corrosive while a cyclohexane-rich product would be less valuable than a product rich in phenol). Therefore, based on the yield of phenol the best catalysts are 20% Ac/CNF, 7.5% Am/CNF, 20% Am/CNF and 20% Am/CNT (see Table 3). Tellingly, the only crystalline phase detected in all these formulations is Mo₂C (or Mo₂C- ζ , which does not seem to behave inherently differently to Mo₂C). This suggests that crystalline Mo₂C is particularly selective to phenol, which is consistent with the fact that catalysts in which Mo₂C is accompanied by MoC—as well as catalysts comprising MoC and/or different molybdenum oxides and catalysts with no crystalline Mo-containing phases—all show lower selectivity to phenol than the catalysts containing Mo₂C or Mo₂C- ζ as their only crystalline phase. Indeed, while the samples containing Mo oxides (*i.e.*, 7.5% Ac/CNT and 20% Ac/CNT) showed high guaiacol conversions, the selectivity to phenol was extremely low, the preferred products being catechol and coke (see Table S2).

Of the samples containing Mo₂C or Mo₂C- ζ as their only crystalline phase, a comparison between the results obtained using 7.5% Am/CNF and 20% Am/CNF is particularly informative, since the only difference between these two catalysts is their metal loading (Mo precursor, carbon support, Mo₂C phase and Mo₂C particle size being all the same). Interestingly, the selectivity to phenol of these two catalysts is virtually identical, the only difference in their behavior being the lower guaiacol conversion shown by 7.5% Am/CNF, which is consistent with the fact that a lower metal loading (at similar dispersion) should translate into a reduced number of active sites.

It is also instructive to compare the results obtained with the 20% Am/CNF and 20% Am/CNT catalysts, these affording very different conversion values (at similar selectivity). In an effort to assess the intrinsic activity of these catalysts, CO chemisorption was applied in order to quantify the concentration of adsorption sites present (see Table 5). Based on their very similar CO uptake, both catalysts have a similar quantity of active sites. Taking this into account and the fact that the guaiacol conversion obtained over 20% Am/CNF was over twice that obtained over 20% Am/CNT, the former formulation appears to be more intrinsically active, although this ignores possible differences in catalyst deactivation due to coke formation.

Table 5. Results of CO chemisorption and intrinsic activity of 20% Am/CNF and 20% Am/CNT.

Catalyst	CO uptake ($\mu\text{mol g}^{-1}$)	Average rate (s^{-1}) ^a
20% Am/CNF	49	0.06
20% Am/CNT	53	0.03

^a Conversion rate normalized to the number of active sites as calculated from CO uptake.

As noted above, the use of CNT as support results in a bimodal particle size distribution containing both micro and nanoparticles in catalysts where carbides are formed, whereas the use of CNF affords solely well-dispersed carbide nanoparticles. In turn, given that these catalysts show a very similar amount of active sites (see Table 5), it follows that the difference in the activity of the 20% Am/CNF and 20% Am/CNT catalysts can be attributed to the effect of particle morphology. Tellingly, spent 20% Am/CNT displayed higher amounts of coke on its surface relative to spent CNF-supported catalysts including 20% Am/CNF (see Table S2), which suggests that this morphology effect can be explained in terms of the catalyst resistance to coking—coke can cover more active sites (and arguably form more

effectively) on a microparticle showing a high concentration of adjacent Mo₂C sites. Therefore, the optimization of particle morphology seems to be a promising way to further improve the performance of molybdenum carbide catalysts.

Finally, a 5% Ru/C reference catalyst was tested under identical reaction conditions for comparison purposes. Albeit this catalyst afforded quantitative guaiacol conversion (the mass balance being 94%), the catalyst displayed 100% selectivity to cyclohexane. Given that (as mentioned above) a cyclohexane-rich product would be less valuable than a product rich in phenol, the CNF-supported Mo₂C catalysts employed in this study represent a promising alternative to the costly Ru-based catalyst commonly used to catalyze this reaction.

2.2.3. Catalyst Testing in an Organic Environment at Different Temperatures

In order to study the effect of temperature on the upgrading of guaiacol in dodecane over Mo₂C/CNF—the formulation showing the best performance (in terms of yield of phenol) at 300 °C—representative CNF-supported catalysts were tested at 350 °C. The catalysts employed in these tests, namely 7.5% Am/CNF and 20% Am/CNF, were chosen in order to study the effect of temperature on two similar catalysts (their only difference being the metal loading) showing noticeably different conversion. In turn, the reaction temperature of 350 °C was chosen based on a recent report by Jongorius *et al.* [2] in which the best results in terms of both guaiacol conversion and phenol selectivity were obtained at this temperature. The results of these experiments are shown in Table 6 and a more comprehensive account of the results of product analysis is given in Table S3 of the Supplementary Materials accompanying this article.

Table 6. Guaiacol upgrading in an organic environment at different temperatures ^a.

Catalyst	Temperature (°C)	Guaiacol conversion (%)	Selectivity to [Yield of] catechol (%)	Selectivity to [Yield of] phenol (%)	Gravimetric mass balance ^b (%)
None	300	7	15 [1]	0 [0]	98
None	350	79	5 [4]	2 [2]	59
7.5% Am/CNF	300	33	9 [3]	38 [12]	98
7.5% Am/CNF	350	99	0 [0]	49 [48]	99
20% Am/CNF	300	53	11 [5.8]	37 [20]	96
20% Am/CNF	350	98	0 [0]	48 [47]	98

^a Reaction conditions: 0.125 g catalyst, 1.25 g guaiacol, 11.25 g dodecane, 580 psi of H₂, 4 h. ^b Mass balances were calculated considering only liquids and solids at the start and the end of the reaction, *i.e.*, mass balance = 100 × (mass of starting reaction mixture)/(mass of recovered liquids and solids). Gaseous reactants and products were omitted from the mass balance calculation for the reasons enumerated in Section 3.5.3.

As mentioned above, the conversion and selectivity values observed in the experiments performed without catalyst can be attributed to thermal effects. Although the guaiacol conversion is considerably higher at 350 °C than at 300 °C in the absence of a catalyst, the selectivity to catechol and phenol remains minimal. Given that very small amounts of products were detected in the liquid product mixture (see Table S3) and a considerably lower mass balance was obtained from the blank experiment performed at 350 °C, it appears that most of the converted guaiacol afforded products in the gas phase which were not

counted in the mass balance calculation. Other authors have explained low mass balances invoking the formation of high molecular weight condensation products not detectable through GC-based methods [2]; however, the fact that in our case mass balances were calculated gravimetrically can be used to rule out this possibility. These results contrast with those obtained in the presence of a catalyst, in which conversions of $\geq 98\%$ and selectivities to phenol approaching 50% were achieved at 350 °C. Tellingly, the mass balances of these reactions were also $\geq 98\%$, which suggests that approximately half of the guaiacol was converted to the coke observed on the spent catalyst surface (see Table S3), to products that were detectable but unidentifiable via GC—which cannot be quantified using GC since their response factors are unknown—and/or to soluble higher molecular weight products undetectable via GC [2], the amount of these products being non-negligible according to a molar mass balance (see Table S4 of the Supplementary Materials). The fact that the performance of both CNF-supported catalysts was almost identical at 350 °C indicates that at this temperature the reaction is fast enough as to be driven to completion by the lower number of active sites present in the 7.5% Am/CNF catalyst. Similarly, the fact that no catechol was detected in the products of the reactions catalyzed at 350 °C suggests that if the conversion of guaiacol into phenol is intermediated by catechol, this reaction was also driven to completion (since phenol presents the most difficult C-O bond to cleave, it is particularly resistant to HDO [7]). Notably, the conversion and selectivity to phenol values obtained at 350 °C over the CNF-supported Mo₂C catalysts are among the best in the literature for carbide catalysts, being comparable to those reported by Jongerius *et al.* [2].

2.3. Catalyst Recycling

The recyclability of the most promising catalyst identified in this study, namely 20% Am/CNF, was assessed by retesting the spent catalyst (after washing and drying) in two additional guaiacol upgrading experiments, which were performed adjusting the amount of solvent and guaiacol to the amount of catalysts recovered (albeit only 8 mg of catalyst was lost during the 2nd run). The spent catalysts were tested without a reactivation step based on the results of Jongerius *et al.* [2], who determined that the recarburation of the spent Mo₂C/CNF catalysts did not afford improved results. The results of these recycling experiments are summarized in Table 7 and a more comprehensive account of the results of product analysis is given in Table S5 of the Supplementary Materials.

It should first be noted that the conversion and selectivity values of fresh 20% Am/CNF in Tables 3 and 7 are somewhat different. Notably, Jongerius *et al.* reported that freshly prepared batches of CNF-supported metal carbide catalysts show some variation in terms of performance, albeit these authors observed different batches of W₂C/CNF to vary considerably and different batches of Mo₂C/CNF to show little variation [2]. However, these authors made these observations at 350 °C, under conditions at which conversion values over Mo₂C/CNF were close to quantitative. Similarly, differences in temperature can be invoked to explain the disparity between the results of the recycling study shown in Table 7 and those obtained by Jongerius *et al.* [2]; in the latter case, no significant loss in guaiacol conversion or selectivity to phenol was observed at 350 °C, while Table 7 shows a $\sim 30\%$ drop in both guaiacol conversion and selectivity to phenol at 300 °C. However, Jongerius *et al.* did observe a 24% drop in conversion and a 20% drop in selectivity to phenol during three sequential (shorter) reactions not showing quantitative conversion [2].

Table 7. Sequential guaiacol upgrading runs in an organic environment over 20% Am/CNF ^a.

Run	Guaiacol conversion (%)	Selectivity to [Yield of] catechol (%)	Selectivity to [Yield of] phenol (%)	Gravimetric mass balance ^b (%)
1	76	2 [2]	50 [38]	98
2	63	3 [2]	36 [23]	97
3	53	5 [3]	36 [19]	98

^a Reaction conditions: 300 °C, 580 psi of H₂, 4 h. Run 1: 0.125 g catalyst, 1.25 g guaiacol, 11.25 g dodecane; Run 2: 0.125 g catalyst, 1.25 g guaiacol, 11.25 g dodecane; Run 3: 0.117 g catalyst, 1.17 g guaiacol, 10.53 g dodecane. ^b Mass balances were calculated considering only liquids and solids at the start and the end of the reaction, *i.e.*, mass balance = 100 × (mass of starting reaction mixture)/(mass of recovered liquids and solids). Gaseous reactants and products were omitted from the mass balance calculation for the reasons enumerated in Section 3.5.3.

In addition, the results shown in Tables 7 and S5 offer some valuable insights regarding catalyst deactivation. Interestingly, although the guaiacol conversion values in Table 7 monotonically decrease in each sequential run, the amount of coke on the spent catalyst surface is also observed to decrease (see Table S5). This suggests that not all of the coke formation taking place during reaction is irreversible, as coke does not appear to accumulate with each subsequent test. This also indicates that there must be another deactivation route in addition to coking, since progressively lower conversion values are obtained in spite of the fact that the amount of coke on the catalyst surface decreases along the experiment sequence. This is in agreement with the conclusions of Jongerius *et al.* who suggested that in addition to irreversible coke formation, the encapsulation of carbide particles in the carbon support represents another potential route of catalyst deactivation [2]. However, more work is necessary to more fully understand the mechanisms of deactivation and to improve catalyst stability and recyclability.

2.4. Guaiacol Upgrading over Mo₂C/CNF in the Presence of Acetic Acid and Furfural

As mentioned in Section 1, guaiacol represents a frequently used model compound for the large number of mono- and dimethoxyphenols resulting from the densification of lignin [3]. However, bio-oil also contains other families of oxygenated compounds stemming from the holocellulosic fraction of biomass, which must be taken into account in bio-oil upgrading studies due to the fact that the reactivity of individual compounds and families of compounds can change when mixed due to synergistic [7] and/or inhibitory [27] effects. With this in mind, a guaiacol upgrading experiment over 20% Am/CNF was performed in the presence of acetic acid and furfural, which are used as model compounds to represent the fractions within bio-oil stemming from hemicellulose and cellulose, respectively [3]. The results of this experiment are summarized in Table 8, and a more comprehensive account of the results of product analysis is given in Table S6 of the Supplementary Materials.

Table 8. Guaiacol upgrading over 20% Am/CNF in the presence of acetic acid and furfural ^a.

Model compound	Conversion (%)	Selectivity to [Yield of] catechol (%)	Selectivity to [Yield of] phenol (%)	Gravimetric mass balance ^b (%)
Guaiacol	6	22 [1]	63 [4]	-
Acetic acid	68	-	-	-
Furfural	80	-	-	-
TOTAL	48	-	-	97

^a Reaction conditions: 0.125 g catalyst, 0.43 g guaiacol, 0.43 g acetic acid, 0.44 g furfural, 11.25 g dodecane, 300 °C, 580 psi of H₂, 4 h. ^b Mass balances were calculated considering only liquids and solids at the start and the end of the reaction, *i.e.*, mass balance = 100 × (mass of starting reaction mixture)/(mass of recovered liquids and solids). Gaseous reactants and products were omitted from the mass balance calculation for the reasons enumerated in Section 3.5.3.

A comparison of the guaiacol conversion values observed over 20% Am/CNF in Tables 3 and 7 clearly illustrates that the presence of acetic acid and furfural greatly inhibits guaiacol conversion. However, it is equally important to note that the presence of acetic acid and furfural greatly augment the selectivity of the catalyst to both catechol and phenol, which may be of interest from an industrial standpoint given that selectivity is commonly prioritized over conversion in industrial processes where any unreacted feed can be recirculated. In stark contrast with the limited conversion of guaiacol, the majority of both acetic acid and furfural were converted, albeit only a small amount of the products observed during the hydrotreatment of these compounds—such as ethyl acetate, THF-MeOH and γ -butyrolactone (see Table S6)—were identified in the liquid product mixture via GC analysis. It is likely that some portion of the acetic acid was converted to ethanol. However, the amount of ethanol produced could not be quantified (due to the interference of ethanol present as a stabilizer in the chloroform used to work up the reaction products). Indeed, the mass balance of this reaction (gravimetric basis) was 97%, which suggests that most of the acetic acid and furfural were converted to solid deposits on the catalyst surface or to liquid organic compounds (as opposed to being converted to gaseous products). Given the relatively low quantities of coke formed during the course of this reaction (see Table S6) it can be inferred that some portion of these reagents were converted to products that were detectable but unidentifiable via GC, and/or to soluble higher molecular weight products undetectable via GC [2]. Using a procedure similar to that described in Table S4, the quantity of unidentified products was found to be approximately 471 mg for this reaction, representing 36% of the feed.

3. Experimental Section

3.1. Catalyst Synthesis

Carbon nanofibers were prepared using a floating catalyst chemical vapor deposition (CVD) method, similar to that described by Martin-Gullon [28] and Weisenberger [29]. Multi-walled carbon nanotubes were produced via the CVD of a xylene/ferrocene feedstock between 750 and 850 °C on quartz substrates [30,31]. The AC employed was Darco KB-G obtained from Sigma Aldrich (St. Louis, MO, USA). Graphitization of the carbon nanotubes was performed at 2700 °C under helium as described elsewhere [25]. Prior to use, the surface area of CNFs and CNTs was increased by an acid treatment in which the support (2 g) was

reacted with 6 M HNO₃ (60 ml) at 80 °C for 3 h under vigorous stirring, after which the solids were filtered, washed with deionized water until the pH of the washings was ~7 and dried at 120 °C. AC did not require pretreatment. Each carbon support was then impregnated with either ammonium molybdate ((NH₄)₆Mo₇O₂₄, Alfa Aesar, Ward Hill, MA, USA) (Am) or molybdic acid (MoO₃ ≥85%, Alfa Aesar, Ward Hill, MA, USA) (Ac) to afford the desired Mo loading (7.5 wt.% or 20 wt.%). The metal loadings were chosen based on previous work by Jongerius *et al.* [2] and Qin *et al.* [15]. The impregnation was carried out by sonicating the support (1 g), deionized water (15 mL) and the prescribed amount of precursor (Am: 0.122 g to afford 7.5 wt.% loading or 0.325 g to afford 20 wt.% loading; Ac: 0.119 g to afford 7.5 wt.% loading or 0.318 g to afford 20 wt.% loading) for 1.5 h. Excess water was removed via rotary evaporation prior to drying in a vacuum oven at 120° C for 14 h. The carbide catalysts employed in this study were prepared via the carbothermal hydrogen reduction (CHR) method [32]. In contrast to the work of Qin and co-workers [15], a carburization temperature of 700 °C proved insufficient to obtain a crystalline carbide phase. Carburization was therefore performed under a flow of 10% H₂/Ar using a ramp rate of 5 °C/min to 1000 °C followed by an isothermal step at this temperature lasting 3 h. After cooling to room temperature, the catalyst was passivated under a flow of 1% O₂/N₂ for 8 h.

3.2. Catalyst Characterization

Powder X-ray diffraction (XRD) measurements were performed on a Phillips X'Pert diffractometer using Cu K α radiation ($\lambda = 1.5406 \text{ \AA}$) and a step size of 0.02°. Average crystallite sizes were calculated using the Scherrer equation. The surface area, pore volume and average pore diameter of the synthesized catalysts were determined by means of N₂ physisorption using a Micromeritics Tristar System at 77 K. N₂ at -196 °C was the sorbate. In all cases samples were degassed overnight at 250 °C prior to the measurements. Total pore volume and pore size distribution were determined using the Density Functional Theory (DFT) method. ICP-OES measurements were performed using a 100 mg sample dissolved in 10 mL of nitric acid. Heating was used to ensure that the sample was completely dissolved. Once cooled, the sample was further diluted to 25 mL with doubly distilled water. Measurements were acquired on a Varian 720-ES spectrometer equipped with a seaspray nebulizer and cyclonic class spray chamber. Parameters include a sample intake of 1 ml/min, Ar plasma flow rate of 15 L/min and an auxiliary gas (Ar) flow rate of 1.5 L/min. The instrument was calibrated using a CRMS manufactured by VHG. CO pulse chemisorption experiments were performed using a Micromeritics AutoChem II 2920 Chemisorption Analyzer. 10% H₂ in Ar (50 mL/min) was flowed through the sample as the temperature was increased to 350 °C at a rate of 5 °C/min followed by a purge under flowing Ar (50 mL/min) while cooling to 35 °C. Ultra high purity CO (99.995% from Matheson-Trigas, Palm, FL, USA) was then pulsed into the system at a volume of 0.5 mL every 2 min until the intensity of the peak was constant. SEM-EDX experiments were conducted on a Hitachi S4800 scanning electron microscope with an Oxford INCA X-MAX EDS/EDX attachment. Samples were placed on carbon tape and inserted into the vacuum chamber uncoated. An emission current of 20 μ A and accelerator voltage of 15 KV was used for these observations. EDX maps were collected at 0–20 KeV.

3.3. Catalyst Testing in Water

Experiments were performed in a mechanically stirred 25 mL stainless steel autoclave. Guaiacol (1.25 g), water (11.25 g), and the catalyst (0.125 g) were simultaneously added to the reactor prior to sealing, after which the reactor was purged with Ar (60 psi), charged to 1000 psi with H₂, mechanically stirred at 500 rpm and heated to the desired temperature. The autoclave temperature was measured by a type-K Omega thermocouple placed inside the reactor body. As soon as the reaction temperature was reached, the pressure was adjusted to 2000 psi. At the completion of the experiment (the reaction time being 4 h), forced air was used to facilitate cooling. Once the reactor reached room temperature, a gas sample was taken for analysis. After opening the reactor, sec-butanol (1.2 g) was added to the product mixture as an internal GC standard. The reaction mixture was then removed by a tared pipette, weighed, and separated by filtration. The catalyst was extracted with acetone to yield additional products. After being allowed to dry under ambient conditions, the filter and recovered solids were weighed again to determine the mass of recovered solids.

3.4. Catalyst Testing in Dodecane

Experiments were performed in a mechanically stirred 25 mL stainless steel autoclave using guaiacol (1.25 g), dodecane (11.25 g), and the catalyst (0.125 g) according to the procedure described in Section 3.3. The initial H₂ charge was 300 psi. As soon as the reaction temperature was reached, the pressure was adjusted to 580 psi. At the end of the reaction, the liquid and solids were separated and the catalyst was extracted with CHCl₃ to yield additional products. Subsequent reactions using a blended feed (1.25 g) of acetic acid, furfural and guaiacol in equal proportions were run in a similar fashion.

3.5. Product Analysis

3.5.1. Liquid Analysis

Cyclohexane (HPLC Grade), ethyl acetate (HPLC Grade, manufactory), furfural (Reagent Grade) and chloroform (HPLC Grade) were purchased from Fisher Scientific. Ethanol (99.5%), cyclopentanone (99+%), cyclopentanol (99%), cyclohexanol (98%), guaiacol (99+%), levulinic acid (98+%) and sec-butanol (99%) were manufactured by Acros Organics (Geel, Belgium). Cyclohexanone (99+%), acetic acid (99.7+%), tetrahydrofurfuryl alcohol (98%), 2-methoxycyclohexanol (99%) and catechol (99%) were purchased from Alfa Aesar (Heysham, UK). γ -Butyrolactone and 1,2-pentanediol were purchased from Sigma-Aldrich (St. Louis, USA). Cyclohexanediol (mixture of *cis*- and *trans*- isomers) was purchased from TCI America (Tokyo, Japan) and phenol (99%) was purchased from City Chemical (West Haven, CT, USA).

Liquid reaction products were analyzed using an Agilent 7890A GC equipped with an Agilent Multimode inlet, a deactivated open ended helix liner and a flame ionization detector (FID). A 0.2 μ L injection was employed and helium was used as the carrier gas. The FID was set to 250 °C with the following gas flow rates: H₂ = 50 mL/min; air = 450 mL/min; makeup = 19 mL/min. The inlet was isothermally maintained at 240 °C in splitless mode. An Agilent J&W DB-Wax column (30 m \times 530 μ m \times 0.5 μ m) rated to 240 °C was employed, maintaining a constant flow of 26 mL/min. The oven

parameters were programmed to start at 35 °C; followed by a ramp of 4 °C/min to 60 °C; followed by a ramp of 10 °C/min to 200 °C; followed by a ramp of 40 °C/min to 240 °C and a 240 °C isotherm lasting 3.75 min. The total run time was 25 min. Chromatographic programming was performed using Agilent Chemstation software. Quantitative calibrations were conducted with solutions prepared according to Table S7 using sec-butanol as the internal standard. Conversion, selectivity and yield were calculated using the following formulas: Guaiacol conversion (%) = $100 \times (\text{mass of guaiacol loaded} - \text{mass of unconverted guaiacol}) / \text{mass of guaiacol loaded}$; Selectivity to specific product (%) = $100 \times \text{mass of the specific product} / (\text{mass of guaiacol loaded} - \text{mass of unconverted guaiacol})$; Yield of specific product (%) = guaiacol conversion \times selectivity to specific product.

3.5.2. Solid Analysis

Attempts were made to study the nature and the amount of the carbonaceous deposits on the surface of spent catalysts by means of thermogravimetric analysis (TGA)—performed under flowing air (50 mL/min) on a TA instruments Discovery Series thermogravimetric analyzer using a temperature ramp of 10 °C/minute from room temperature to 800 °C. However, these efforts proved unfruitful due to the fact that the weight loss associated with coke combustion could not be deconvoluted from the weight loss stemming from the combustion of the carbon supports (which were studied separately by subjecting fresh catalyst to TGA).

3.5.3. Gas Analysis

An Agilent 3000 Micro-GC with a configuration previously reported [33] was calibrated for possible gaseous products, including straight chain C1-C6 alkanes and alkenes. The analysis of gaseous products formed during representative guaiacol experiments proved unremarkable, no products being detected.

4. Conclusions

In this work the hydrodeoxygenation of guaiacol over molybdenum carbides supported on three types of carbon support—activated carbon, multi-walled carbon nanotubes, and carbon nanofibers—was studied. The use of activated carbon as support afforded an X-ray amorphous Mo phase, whereas crystalline carbide phases were obtained on carbon nanofibers and, in some cases, on carbon nanotubes. Scanning electron micrographs revealed the presence of large molybdenum carbide particles ($>2 \mu\text{m}$) in the CNT-supported catalysts containing molybdenum carbide phases, whereas in the CNF-supported samples molybdenum carbide was exclusively present in the form of nanoparticles. In the HDO of guaiacol in dodecane, catechol and phenol were obtained as the main products, although in some instances cyclohexane was also formed. The fact that catechol was observed in all reaction mixtures suggests that guaiacol is converted into phenol via sequential demethylation and HDO, albeit the simultaneous occurrence of a direct demethoxylation pathway cannot be discounted. Based on the yield of phenol obtained, 20% Ac/CNF, 7.5% Am/CNF, 20% Am/CNF and 20% Am/CNT were identified as the best catalysts; notably, the only crystalline phase detected in all these formulations was Mo₂C (or Mo₂C- ζ , which does not seem to behave inherently differently to Mo₂C), indicating that crystalline Mo₂C is particularly selective to phenol. At 350 °C, CNF-supported Mo₂C afforded near quantitative guaiacol

conversion ($\geq 98\%$), with a selectivity to phenol approaching 50%. When guaiacol HDO was performed using 20%Am/CNF in the presence of acetic acid and furfural, the conversion of guaiacol was greatly inhibited, although the selectivity of the catalyst to both catechol and phenol was increased.

Acknowledgments

This work was supported by a Seed Grant of the University of Kentucky Center for Applied Energy Research (UK CAER). Renan Sales is thanked for technical assistance. Ashley Morris, John Craddock and Matthew Weisenberger of the UK CAER Carbon Materials group are thanked for providing the nanostructured carbons employed in this work.

Author Contributions

E.S.-J., R.P. and M.C. conceived and designed the experiments; M.P., R.P. and T.M. performed the experiments; E.S.-J., M.P., R.P., T.M. and M.C. analyzed the data; E.S.-J., R.P., T.M. and M.C. wrote the paper.

Conflicts of Interest

The authors declare no conflict of interest. The founding sponsors had no role in the design of the study; in the collection, analyses, or interpretation of data; in the writing of the manuscript, and in the decision to publish the results.

References

1. Zakzeski, J.; Bruijninx, P.C.A.; Jongerius, A.L.; Weckhuysen, B.M. The Catalytic Valorization of Lignin for the Production of Renewable Chemicals. *Chem. Rev.* **2010**, *110*, 3552–3599.
2. Jongerius, A.L.; Gosselink, R.W.; Dijkstra, J.; Bitter, J.H.; Bruijninx, P.C.A.; Weckhuysen, B.M. Carbon nanofiber supported transition-metal carbide catalysts for the hydrodeoxygenation of guaiacol. *ChemCatChem* **2013**, *5*, 2964–2972.
3. Elliott, D.C.; Hart, T.R. Catalytic Hydroprocessing of Chemical Models for Bio-oil. *Energy Fuels* **2009**, *23*, 631–637.
4. Lin, Y.-C.; Li, C.-L.; Wan, H.-P.; Lee, H.-T.; Liu, C.-F. Catalytic Hydrodeoxygenation of Guaiacol on Rh-Based and Sulfided CoMo and NiMo Catalysts. *Energy Fuels* **2011**, *25*, 890–896.
5. Jongerius, A.L.; Jastrzebski, R.; Bruijninx, P.C.A.; Weckhuysen, B.M. CoMo sulfide-catalyzed hydrodeoxygenation of lignin model compounds: An extended reaction network for the conversion of monomeric and dimeric substrates. *J. Catal.* **2012**, *285*, 315–323.
6. Gutierrez, A.; Kaila, R.K.; Honkela, M.L.; Slioor, R.; Krause, A.O.I. Hydrodeoxygenation of guaiacol on noble metal catalysts. *Catal. Today* **2009**, *147*, 239–246.
7. Graça, I.; Lopes, J.M.; Cerqueira, H.S.; Ribeiro, M.F. Bio-oils Upgrading for Second Generation Biofuels. *Ind. Eng. Chem. Res.* **2013**, *52*, 275–287.
8. Furimsky, E. Catalytic hydrodeoxygenation. *Appl. Catal. A* **2000**, *199*, 147–190.
9. Wang, H.; Male, J.; Wang, Y. Recent Advances in Hydrotreating of Pyrolysis Bio-Oil and Its Oxygen-Containing Model Compounds. *ACS Catal.* **2013**, *3*, 1047–1070.

10. Levy, R.B.; Boudart, M. Platinum-like behavior of tungsten carbide in surface catalysis. *Science* **1973**, *181*, 547–549.
11. Gao, Q.; Zhang, C.; Xie, S.; Hua, W.; Zhang, Y.; Ren, N.; Xu, H.; Tang, Y. Synthesis of Nanoporous Molybdenum Carbide Nanowires Based on Organic–Inorganic Hybrid Nanocomposites with Sub-Nanometer Periodic Structures. *Chem. Mater.* **2009**, *21*, 5560–5562.
12. Han, J.; Duan, J.; Chen, P.; Lou, H.; Zheng, X. Molybdenum Carbide-Catalyzed Conversion of Renewable Oils into Diesel-like Hydrocarbons. *Adv. Synth. Catal.* **2011**, *353*, 2577–2583.
13. Chang, J.; Danuthai, T.; Dewiyanti, S.; Wang, C.; Borgna, A. Hydrodeoxygenation of Guaiacol over Carbon-Supported Metal Catalysts. *ChemCatChem* **2013**, *5*, 3041–3049.
14. Han, J.; Duan, J.; Chen, P.; Lou, H.; Zheng, X.; Hong, H. Carbon-Supported Molybdenum Carbide Catalysts for the Conversion of Vegetable Oils. *ChemSusChem* **2012**, *5*, 727–733.
15. Qin, Y.; Chen, P.; Duan, J.; Han, J.; Lou, H.; Zheng, X.; Hong, H. Carbon nanofibers supported molybdenum carbide catalysts for hydrodeoxygenation of vegetable oils. *RSC Adv.* **2013**, *3*, 17485–17491.
16. Hollak, S.A.W.; Gosselink, R.W.; van Es, D.S.; Bitter, J.H. Comparison of Tungsten and Molybdenum Carbide Catalysts for the Hydrodeoxygenation of Oleic Acid. *ACS Catal.* **2013**, *3*, 2837–2844.
17. Stellwagen, D.R.; Bitter, J.H. Structure-performance relations of molybdenum- and tungsten carbide catalysts for deoxygenation. *Green Chem.* **2015**, *17*, 582–593.
18. Han, J.; Duan, J.; Chen, P.; Lou, H.; Zheng, X.; Hong, H. Nanostructured molybdenum carbides supported on carbon nanotubes as efficient catalysts for one-step hydrodeoxygenation and isomerization of vegetable oils. *Green Chem.* **2011**, *13*, 2561–2568.
19. Escalona, N.; Aranzuez, W.; Leiva, K.; Martínez, N.; Pecchi, G. Ni nanoparticles prepared from Ce substituted LaNiO₃ for the guaiacol conversion. *Appl. Catal. A* **2014**, *481*, 1–10.
20. Mortensen, P.M.; Gardini, D.; de Carvalho, H.W.P.; Damsgaard, C.D.; Grunwaldt, J.-D.; Jensen, P.A.; Wagner, J.B.; Jensen, A.D. Stability and resistance of nickel catalysts for hydrodeoxygenation: carbon deposition and effects of sulfur, potassium, and chlorine in the feed. *Catal. Sci. Technol.* **2014**, *4*, 3672–3686.
21. Zhang, X.; Long, J.; Kong, W.; Zhang, Q.; Chen, L.; Wang, T.; Ma, L.; Li, Y. Catalytic Upgrading of Bio-oil over Ni-Based Catalysts Supported on Mixed Oxides. *Energy Fuels* **2014**, *28*, 2562–2570.
22. Olcese, R.N.; Bettahar, M.; Petitjean, D.; Malaman, B.; Giovanella, F.; Dufour, A. Gas-phase hydrodeoxygenation of guaiacol over Fe/SiO₂ catalyst. *Appl. Catal. B* **2012**, *115–116*, 63–73.
23. Olcese, R.; Bettahar, M.M.; Malaman, B.; Ghanbaja, J.; Tibavizco, L.; Petitjean, D.; Dufour, A. Gas-phase hydrodeoxygenation of guaiacol over iron-based catalysts. Effect of gases composition, iron load and supports (silica and activated carbon). *Appl. Catal. B* **2013**, *129*, 528–538.
24. Olcese, R.N.; Francois, J.; Bettahar, M.M.; Petitjean, D.; Dufour, A. Hydrodeoxygenation of Guaiacol, A Surrogate of Lignin Pyrolysis Vapors, Over Iron Based Catalysts: Kinetics and Modeling of the Lignin to Aromatics Integrated Process. *Energy Fuels* **2013**, *27*, 975–984.
25. Andrews, R.; Jacques, D.; Qian, D.; Dickey, E.C. Purification and structural annealing of multiwalled carbon nanotubes at graphitization temperatures. *Carbon* **2001**, *39*, 1681–1687.

26. Gosselink, R.W.; Van Den Berg, R.; Xia, W.; Muhler, M.; De Jong, K.P.; Bitter, J.H. Gas phase oxidation as a tool to introduce oxygen containing groups on metal-loaded carbon nanofibers. *Carbon* **2012**, *50*, 4424–4431.
27. Jackson, M.A. Ketonization of model pyrolysis bio-oil solutions in a plug-flow reactor over a mixed oxide of Fe, Ce, and Al. *Energy Fuels* **2013**, *27*, 3936–3943.
28. Martin-Gullon, I.; Vera, J.; Conesa, J.A.; González, J.L.; Merino, C. Differences between carbon nanofibers produced using Fe and Ni catalysts in a floating catalyst reactor. *Carbon* **2006**, *44*, 1572–1580.
29. Weisenberger, M.; Martin-Gullon, I.; Vera-Agullo, J.; Varela-Rizo, H.; Merino, C.; Andrews, R.; Qian, D.; Rantell, T. The effect of graphitization temperature on the structure of helical-ribbon carbon nanofibers. *Carbon* **2009**, *47*, 2211–2218.
30. Craddock, J.D.; Weisenberger, M.C. Harvesting of large, substrate-free sheets of vertically aligned multiwall carbon nanotube arrays. *Carbon* **2015**, *81*, 839–841.
31. Andrews, R.; Jacques, D.; Rao, A.M.; Derbyshire, F.; Qian, D.; Fan, X.; Dickey, E.C.; Chen, J. Continuous production of aligned carbon nanotubes: a step closer to commercial realization. *Chem. Phys. Lett.* **1999**, *303*, 467–474.
32. Liang, C.; Ying, P.; Li, C. Nanostructured β -Mo₂C Prepared by Carbothermal Hydrogen Reduction on Ultrahigh Surface Area Carbon Material. *Chem. Mater.* **2002**, *14*, 3148–3151.
33. Morgan, T.; Santillan-Jimenez, E.; Harman-Ware, A.E.; Ji, Y.; Grubb, D.; Crocker, M. Catalytic deoxygenation of triglycerides to hydrocarbons over supported nickel catalysts. *Chem. Eng. J.* **2012**, *189–190*, 346–355.

© 2015 by the authors; licensee MDPI, Basel, Switzerland. This article is an open access article distributed under the terms and conditions of the Creative Commons Attribution license (<http://creativecommons.org/licenses/by/4.0/>).